Slow and swift heavy ions irradiation of zirconium nitride (ZrN) and the migration behaviour of implanted Eu

T.F. Mokgadi[1], M.J. Madito[2], M. Mlambo[1], V.A. Skuratov[3,4,5], S.V. Mtloung[6,7]and T.T. Hlatshwayo[1*]

[1]Physics Department, University of Pretoria, Private Bag X20, 0028 Hatfield, South Africa

[2]iThemba LABS, National Research Foundation, PO Box 722, Somerset West 7129, Cape Town, South Africa

[3]Joint Institute for Nuclear Research, Dubna, Russia

[4]National Research Nuclear University MEPhI, Moscow

[5]Dubna State University, Dubna, Moscow Region, Russia

[6]Department of Physics, Nelson Mandela University (NMU), Port Elizabeth 6031, South Africa

[7]Department of Physics, Sefako Makgatho Health Science University, Medunsa, 0204, South Africa

*corresponding author, TT Hlatshwayo. e-mail address: thulani.hlatshwayo@up.ac.za

Abstract

Zirconium nitrate (ZrN) layers of about 20 μm were deposited onto silicon (Si) substrates at room temperature (RT) using a vacuum arc deposition technique. Some of the as-deposited samples were irradiated with Eu (360 keV) to a fluence of 1.0×10^{16} cm^{-2} at RT. Others were irradiated with 167 MeV Xe ions to the fluence of 6.7×10^{14} cm^{-2} at RT. Both Eu and Xe irradiated samples were annealed at 800 and 900 ^{o}C for 5 hours. The as-deposited samples were characterised by x-ray diffraction (XRD) and Raman spectroscopy while irradiated and annealed samples were characterised by Raman spectroscopy and Rutherford backscattering spectrometry (RBS). XRD results showed (111), (200), (311) and (222) planes of ZrN confirming the polycrystalline nature as-deposited layers Raman results of as-deposited ZrN showed all vibration modes indicating ZrN with defects. Irradiation with slow ions resulted in the accumulation of defects in the irradiated samples. Fewer defects were observed in the swift heavy ions irradiated samples. Thermal annealing at 800 and 900 ^{o}C resulted in different stoichiometric structures of ZrN with broken octahedral symmetry. No migration of implanted Eu was observed after annealing at these temperatures.

Introduction

The driving factor for the information age is high consumption and reliance on electrical energy. The industrialization of the developed economies and global move to significant decrease of the carbon footprint are two major conflicting features influencing the global energy economy. As of 2016, 38.3% of the world's electricity generation has been from coal, 23.1% gas and only 10.4% from nuclear [1]. Although coal-and-gas powered plants are cheaper to design and build, making them attract intense interest in developing countries, their long-term cost of use, however, is ever increasing. Nuclear power production in the world in 2017 contributed 2487 TWh of electricity, up from 2477 in 2016 [2] with about 450 nuclear power reactors, and 60 more under construction, equivalent to about 15% of existing capacity [2]. As a result, huge amounts of radioactive waste are generated yearly. In an attempt to reduce the toxic nuclear waste, inert matrix fuels (IMF) have been advanced to transmute the transuranic elements [3, 4]. IMF's such as the nitrides and carbides have been suggested as suitable materials for fast neutronic systems [4]. Zirconium nitride (ZrN) has exceptional physical and chemical properties, such as the high melting point, thermal conductivity and perfect solubility for minor actinide (MA: Np, Am, Cm) elements, making it possible to directly burnup plutonium or transmuting long-lived actinides in an accelerator-driven sub-critical system (ADS) or a fast reactor (FR) [5,6,7]. ZrN is also a possible candidate for the fuel phase in generation IV Gas-cooled Fast Reactors (GFR) [5,8]. The NaCl-like structure of ZrN reveals a wide range of non-stoichiometry nature which may alter its electronic structure, vacancy concentration and structural stability during irradiation [5,9]. In nuclear reactors, ZrN will be subjected to different irradiations including ions of different energies and neutrons at elevated temperatures. Under these conditions, ZrN needs to retain fission products. Irradiation may compromise the integrity of ZrN. Hence it is important to understand the irradiation behaviour of ZrN and migration behaviour of fission products. Several studies have been performed in investigating the irradiation tolerance of ZrN [10-18]. These were done by both slow ions and swift heavy ions at different irradiation temperatures up to 200 displacements per atom (dpa) [10]. Under all previous irradiation conditions, no amorphization of ZrN was observed indicating irradiation tolerance of ZrN. Very little has been reported on the migration of fission products in ZrN with the exception of He [11].

In this study, swift heavy and slow ion irradiation behaviour of ZrN deposited onto Si substrates was investigated by Raman spectroscopy. Xenon (Xe) ions of 167 MeV and Europium (Eu) ions of 360 keV were individually implanted into ZrN all to a fluence of

6.7×10^{14} cm^{-2} and 1×10^{16} cm^{-2} at room temperature (RT), respectively. The annealing of radiation damage together with migration of implanted Eu was investigated at 800 and 900 ^{o}C using Raman spectroscopy and RBS, respectively.

Experimental methods

Zirconium nitride (ZrN) of about 20 μm thickness was deposited on silicon (Si) substrates using vacuum arc deposition at Belarussian State University, Minsk, Belarus. Some of the as-deposited samples were implanted with Eu ions at room temperature (RT). The implantation energy was 360 keV and the fluence was 1.1×10^{16} cm^{-2}. Other samples were irradiated with Xe ions of 167 MeV to a fluence of 6.77×10^{14} cm^{-2} also at RT. The Eu (360 keV) ions implantation were done at the Friedrich-Schiller-University Jena, Germany. Swift heavy ions (SHI) (Xe (167 MeV)) were irradiated using IC-100 cyclotron at the Flerov laboratory on nuclear reactions (FLNR), Joint Institute for nuclear research (JINR), Dubna, Russia.

The Eu implanted samples were then isochronally annealed in vacuum using the computer controlled *Webb 77* graphite furnace at 800 and 900 ^{o}C for 5 hours. The as-deposited samples were characterised by x-ray diffraction (XRD) and Raman spectroscopy. The implanted, irradiated and annealed samples were characterised by Raman spectroscopy and Rutherford Backscattering Spectrometry (RBS). XRD was performed using the PANalytical X'Pert Pro powder diffractometer with the X'Celerator detector and variable divergence and fixed receiving slits with Fe filtered Co-Kα radiation with the wavelength of 1.789 Å. The phases were identified using X'Pert Highscore plus software. Raman spectroscopy was performed using the Witec alpha 300 RAS+ Raman spectrometer. Acquisition of image scans was carried out using a 532 nm excitation laser at a power of 15 mW and a 50×/0.75 numeric aperture objective with a spot size of 433 nm. The cross-section image scans were acquired over 40×40 μm^2 area with 150 points per line and 150 lines per image using the integration time of 1s. Cross-sectional measurements were done on the swift heavy ions irradiated samples on an uneven cross-sectional surface and characterised with cluster analysis (distribution maps). RBS was performed at room temperature with helium (He^{+}) beam at the energy of 1.8 MeV with a scattering angle of 165^{o}. 8μC was collected per measurement to improve statistics. The RBS Eu profiles in energy-channels were converted into depth in nm using energy loss data and the theoretical ZrN density of 8.264×10^{22} atcm-3. Both implantation and irradiation experiments were simulated using full cascade SRIM-2012

calculations [19], the displacement of 35 eV and 25 eV were used for Zr and N, respectively [17].

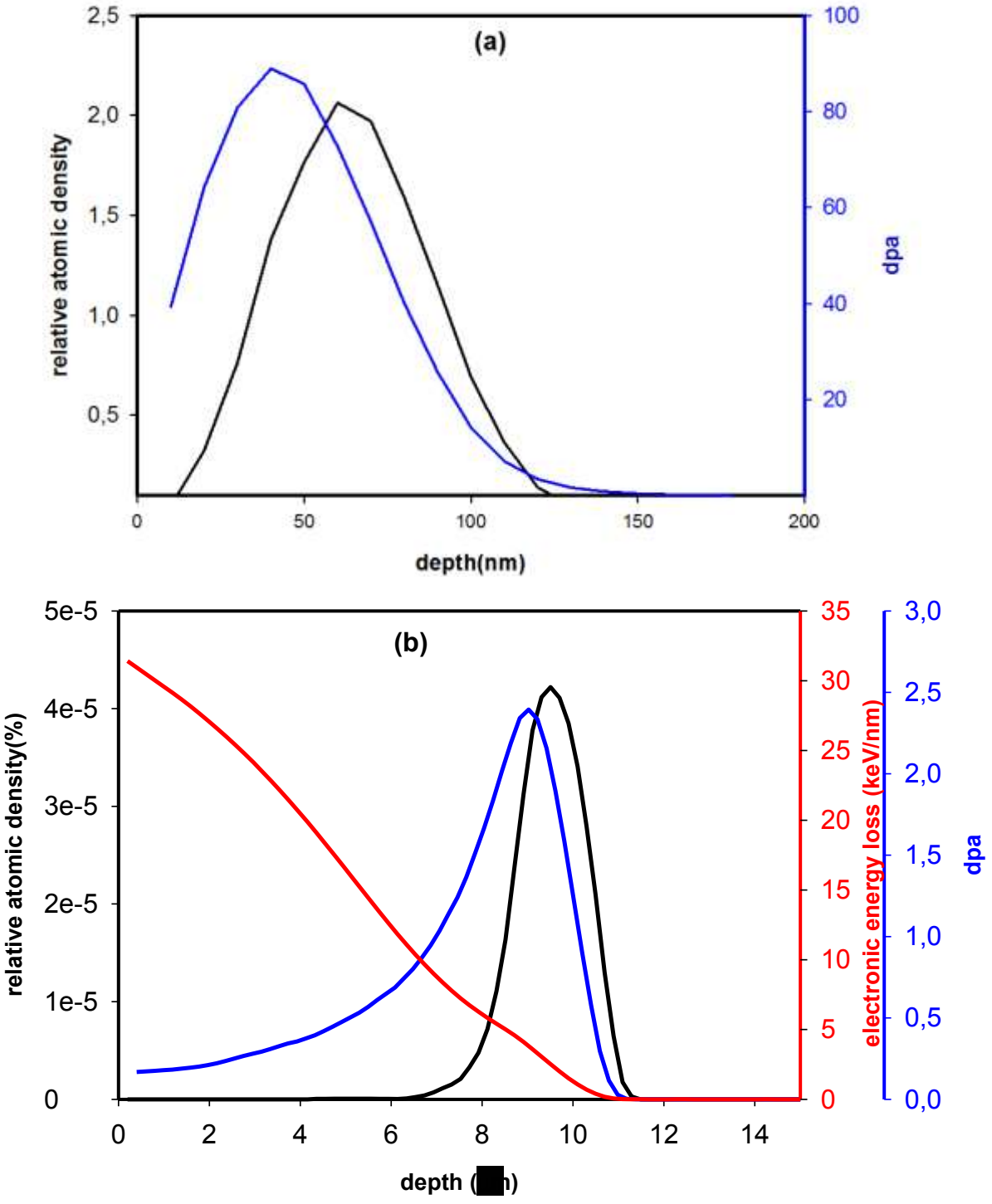

Fig. 1: SRIM simulated profiles of Eu ions of 360 keV (a) and Xe ions of 167 MeV (b) irradiated into ZrN. The relative atomic density is shown in black, displacement per atom (dpa) in blue and electronic energy loss in red.

Results and discussion

Fig 1 shows the simulated results of Xe (167 MeV) and Eu (360 keV) ions irradiated into ZrN. Low energy Eu ions resulted in the projected range (Rp) of about 60 nm from the ZrN surface with more defects created closer to the surface (with the maximum dpa of about 90 at 40 nm). The electronic and nuclear energy loss were found to be 0.8 and 5 kev/nm at the surface, respectively. SHI irradiation resulted in the projected range (Rp) of about 10 μm from the ZrN surface with maximum dpa of about 2.5 at 9 μm. The electronic and nuclear energy loss were found to be 30 and 0.14 keV/nm at the surface, respectively. These show that irradiation with low energy ions subjected the ZrN surface to nuclear energy loss while SHI irradiation subjects the surface to electronic energy loss.

The XRD spectrum of the as-deposited ZrN is shown in Fig 2. The peaks at position 2θ of 39.499º, 45.932º, 80.640º, and 84.036º were found to correspond to (111), (200), (311) and (222) ZrN planes, respectively. Using the (111) plane, the average crystal size of about 10 nm was obtained from Scherrer's equation. This indicated the nanocrystalline nature of the deposited ZrN layer. The peak at the position 2θ of about 82.338º was found to be silicon (Si) (100) indicating that the X-ray penetrated the ZrN deposited layer.

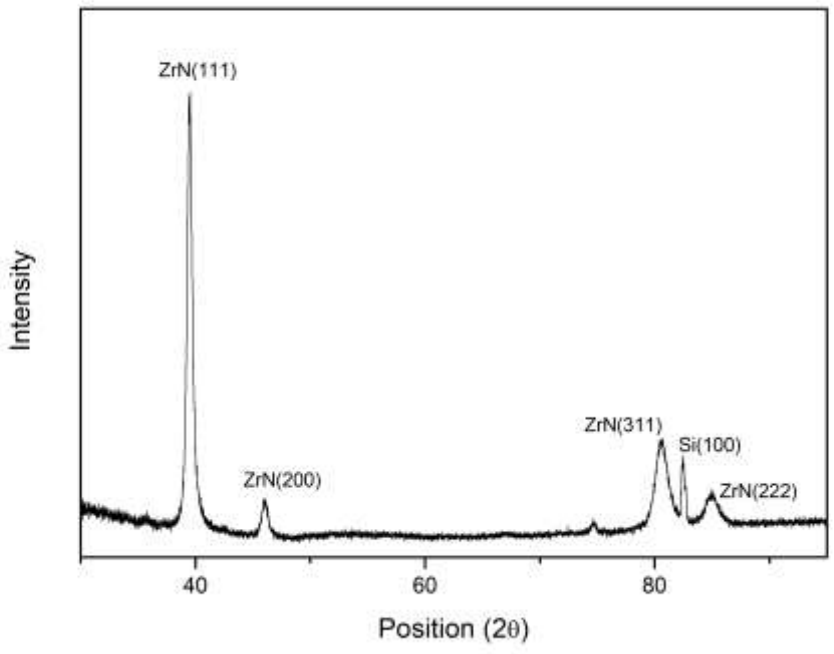

Fig. 2: XRD spectrum of ZrN deposited on the Si substrate.

Raman spectroscopy is used to render valuable information about order/disorder changes, defect density, stress, and grain size of the deposited layers [20, 21, 22]. Defect-free ZrN has the face-centered cubic NaCl structure with every atom at the site of inversion symmetry (octahedral site symmetry), and therefore presenting no vibrational modes. However, the presence of vacancies perturbs the octahedral symmetry allowing the appearance of Raman-active modes [23]. The theory of how 'defect' induced first-order phonon modes arise is well established [24, 25]. Fig. 3 shows the Raman spectrum of as-deposited ZrN. Two acoustic modes, transverse (TA) at 169 cm^{-1} and longitudinal (LA) at 230 cm^{-1}, an optical transverse mode (TO) at about 457 cm^{-1} and a shoulder corresponding to the optical longitudinal mode (LO) at about 510 cm^{-1} are observed. There are two peaks in the region 300-410 cm^{-1} between the acoustic and optic modes, which are low-frequency second-order acoustic modes (2A): 2TA at 338 cm^{-1} and TA+LA at 407 cm^{-1}. The acoustic modes are characteristic of zirconium vacancies while the optical modes characterize the N vacancies [26, 27]. The appearance of second-order acoustic modes is an indication of ZrN with less stoichiometric defects [26].

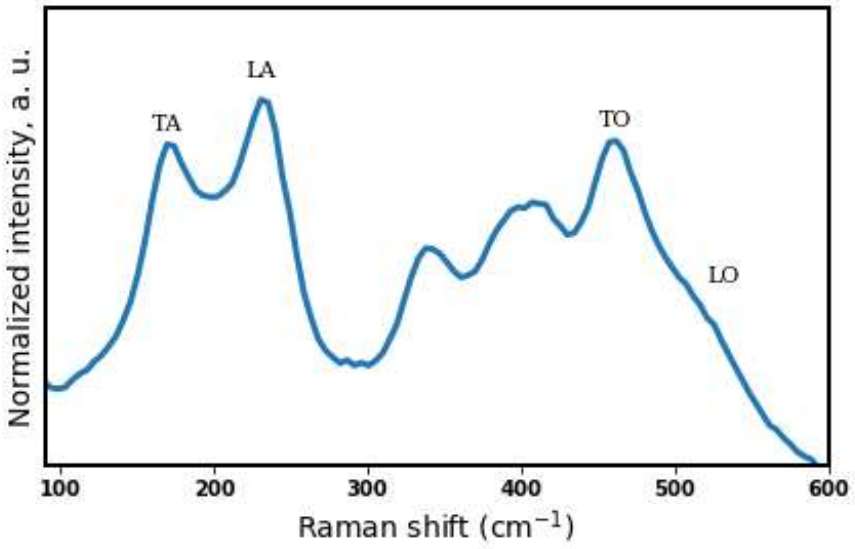

Fig. 3: Raman spectrum of as-deposited ZrN

Fig. 4(a) shows the Raman spectra of ZrN implanted with Eu ions, the as-deposited spectrum is given for comparison. Irradiation with low energy ions caused the increase in the TA and LA intensity modes. This was accompanied by peak shifts of TA mode from 169 to 174 cm^{-1}. The LA mode blue-shifted from 230 to 226 cm^{-1}. The other noticeable feature was the partial

filling of the gap between TA and LA modes signifying the increase in the concentration of point defects in the implanted sample (Fig 4(b)). Fig 4(a) also shows a significant decrease in the intensity of the TO peak, accompanied by a red-shift from 457 to 494 cm^{-1} for the Eu implanted sample. This attests to the creation of point defects, specifically N vacancies. Furthermore, there is a combination of the two 2A modes in the region 300-410 cm^{-1}, which could be due to increase of stoichiometric defects [26]. There is also a disappearance of the shoulder due to LO mode. These changes are due to the accumulated radiation defects. Similar changes have been reported due to accumulation of vacancies in TiC [28]. To get more insight in the radiation damage/defects retained after implantation, the full-width at half-maximum (FWHM) of TO modes were calculated as shown in Fig 4 (c) and (d). The FWHM of implanted sample was 65.56 in Fig 4(d) compared to FWHM for a virgin of 49.06 cm^{-1} in Fig 4 (c). The widening of the TO mode further indicates accumulation of defects. Similar irradiation behaviour has been reported in [29] where ZrN was irradiated with Xe ions of 360 keV to a fluence of 5×10^{16} cm^{-2} at RT and transmission electron microscopy (TEM) analyses indicated minor changes in the implanted ZrN.

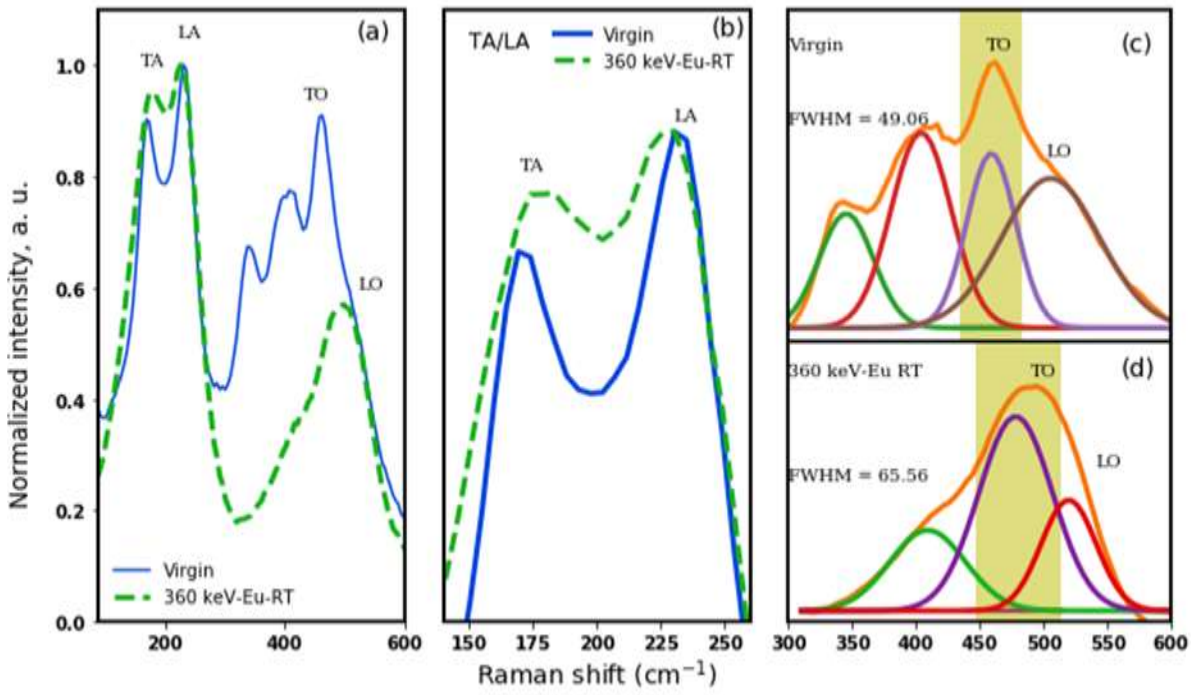

Fig. 4: The surface Raman spectra of ZrN implanted with (a) Eu ions at 360 keV RT,(b) TA and LA modes, (c) and (d) deconvoluted spectra of optical modes with the FWHM of the TO modes. The Raman spectrum of pristine ZrN is included for comparison.

Fig. 5(a) shows the surface Raman spectrum of ZrN irradiated with SHI (Xe ions of 167 MeV), the virgin spectrum is included for comparison. Irradiating with SHI resulted in the reduction in the peak intensities of all modes except the LA intensity mode remaining the same. The only peak shifts observed was the TO mode to 480 cm^{-1}, indicating an increased lattice disorder around N atoms. This was accompanied by a decrease in the intensity of the two second-order acoustic modes between 300-410 cm^{-1} region and the broadening of TO mode. Similar results have been reported on ZrN irradiated with similar SHI and were explained to be due to point defects formed through a high density electronic excitations of ZrN via thermal spike model [23]. Comparing the Raman results of low energy ions and SHI irradiated ZrN, it is quite evident that low energy ion-irradiated ZrN had more defects. This is due to higher nuclear energy loss of the slow ions, which results in the creation of more vacancies. The created vacancies have less energy to move around which reduces the probability of recombination with their original sites during implantation performed at RT. During SHI irradiation, fewer vacancies are generated as a result of low nuclear energy loss while the excess of electronic energy loss provides energy to the existing vacancies to move around which leads to higher probability of recombination. Since N has a smaller displacement energy than Zr, more N vacancies are expected to be dominant in both implantation and irradiation.

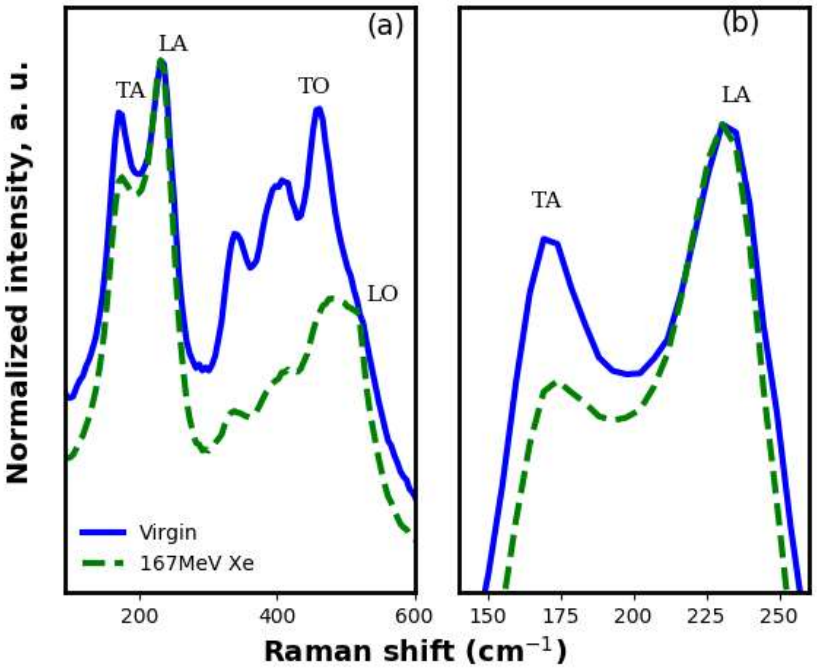

Fig 5: Raman spectra of ZrN irradiated with 167 MeV ions with virgin for comparison (a), TA and LA modes (b).

Fig. 6 shows cross-sectional optical microscope images of virgin and SHI irradiated samples, superimposed by cluster images (distribution maps) in Fig 6 (a) and (c). The average Raman spectra shown correspond to each colour on the overlay cluster images. The cluster images in Fig. 6 (b) and (d) shows the cross-section of average damage region of the swift heavy ion irradiation. On the deposited ZrN of about 20 µm, SHI irradiation caused the damage from the surface to about 10 µm into the sample. The damage on the surface is due to the electronic energy loss induced by the inelastic collisions that may be created close to the ion tracks. The electronic energy loss dominates to about 10 keV/nm at a depth of around 7 µm (fig. 1(b)). The atomic collisions due to the nuclear energy loss begin at around 7 µm depth until maximum collisions at around 10 µm where maximum point defects concentrations are created. These results clearly demonstrate the power of cross–sectional Raman in characterizing the damage retained by SHI without destroying the samples.

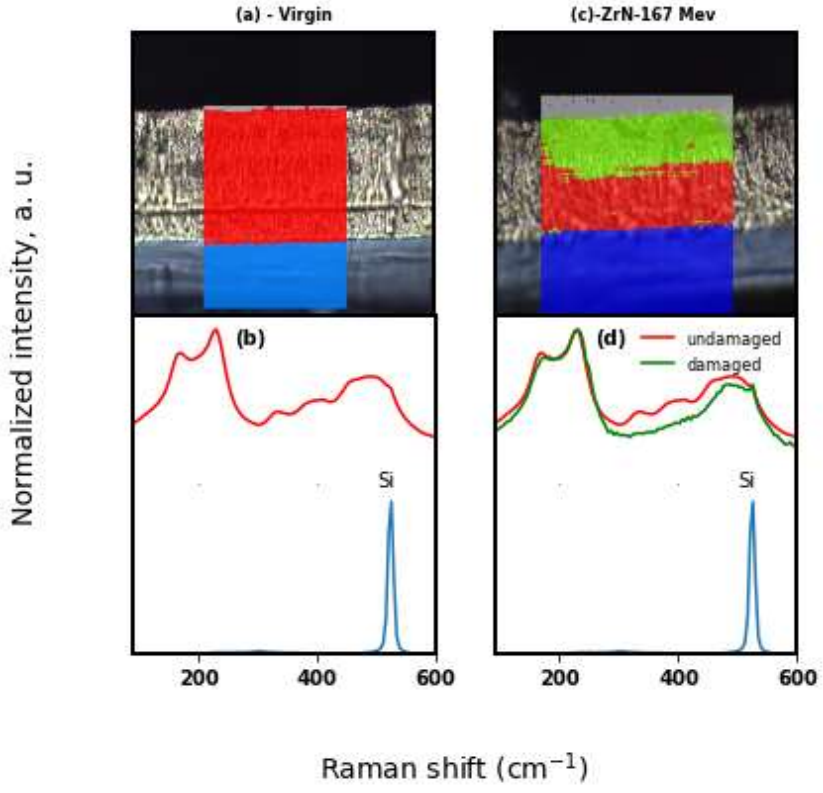

Fig. 6: (a, c) Cross-sectional optical microscope images superimposed by cluster images (distribution maps). (b, d) The average Raman spectra corresponding to each colour on the overlay cluster images

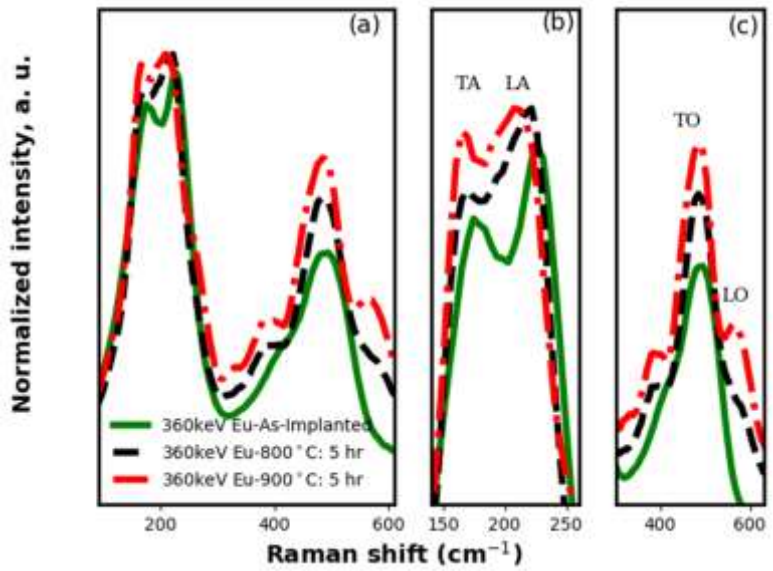

Fig. 7: Raman spectra comparing (a) the defects on annealed and the as-implanted sample with europium (Eu) ions at 360 keV-RT , annealed isochronically at 800 and 900 °C for 5 hours, (b) the TA and LA modes and (c) the first-order optic modes

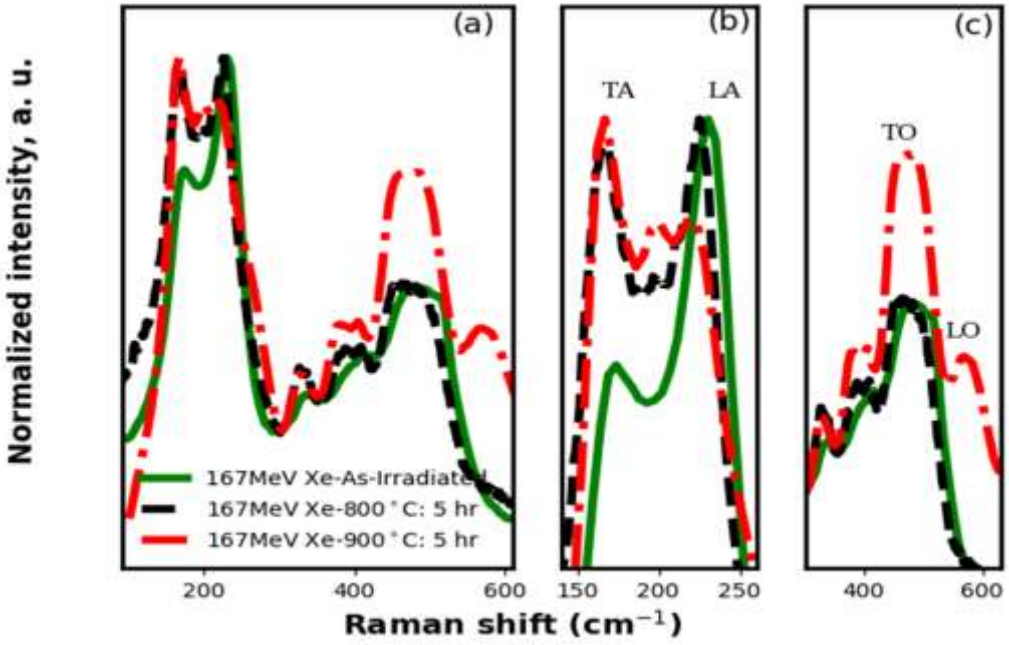

Fig. 8: Raman spectra comparing (a) the defects on annealed and the as-implanted sample with Xenon (Xe) ions at 167 MeV-RT , annealed isochronically at 800 and 900 °C for 5 hours, (b) the TA and LA modes and (c) the first-order optic modes

The thermal stability of radiation damage was assessed in Eu implanted and Xe irradiated ZrN after annealing the samples at 800 and 900 °C for 5 hours. Raman spectra of the Eu implanted then annealed samples are shown in Fig. 7. There is a slight shift to lower

frequencies of the TA and LA modes and the closing of the gap between TA and LA modes in Fig 7(b) as the annealing temperature increases. Thermal annealing at 800 and 900 ^{o}C, also resulted in a slight shift of the TO peak to about 485 cm^{-1} from 494 cm^{-1} and peak intensity increased. These were accompanied by the reappearance of the peaks centered at 400 cm^{-1} and the LO mode shoulder around 560 cm^{-1}. The continuous closing of the gap between the TA and LA modes and the increase in their intensities suggest an increase in N vacancies while the increase in the intensity of the TO mode and reappearance of the LO mode suggests a recombination of the N atoms with their vacant sites. The simultaneous increase and recombination might be suggesting creation of N_{Zr} antisite defects with some N atoms occupying the Zr atom sites at the same time others combining with their vacancies. Similar behaviour has been reported for other ceramics with the same structure–HfN [30] where the concentration of N vacancies was varied and the formation of N_{Hf} antisites was reported. The reappearance of one of the second-order acoustic modes might point to the lowering of point defect concentration as a result to thermal annealing.

Raman spectra of Xe irradiated and then annealed samples are shown in fig. 8. Thermal annealing at 800 ^{o}C resulted in the appearance of a peak between TA and LA at around 200 cm^{-1}. This is accompanied by an increase in the intensity of the TA mode. These suggest that a reduction in the N vacancy concentration. The slight increase in the intensity of the second-order acoustic modes and a slight narrowing of the optical mode (fig. 8 (b)) also confirmed the reduction in N vacancy concentration. Annealing at 900 ^{o}C resulted in the increase in the intensity of the peak between TA and LA at around 200 cm^{-1}, the LA intensity decreased while the TA stays the same. The second-order acoustic modes were well-pronounced after annealing at 900 ^{o}C. The TO intensity also increased and the LO became more pronounced. Similar to the implanted samples, these changes indicate the reduction of N vacancies while the appearance of more secondary modes indicates less vacancies in the latter samples. The difference in the annealing results could be explained by more vacancies in the implanted compared to irradiated samples. The influence of Eu in the implanted samples might also have influence in the annealing of vacancies as it will be discussed below. The difference in the annealed Raman spectra compared to the pristine spectrum might indicate that annealing of the Eu implanted and Xe irradiated ZrN at these temperatures results in ZrN that is stoichiometrically different to pristine ZrN structure.

The migration of Eu implanted into ZrN was monitored by RBS after each annealing step. Due to the limitation in the maximum analysing energy of our RBS system, the Eu profile

could not be entirely separated from Zr. The Eu was extracted by subtracting the normalised un-implanted RBS spectrum from implanted and implanted then annealed samples. RBS data in energy-channels were converted into depth using energy loss factor and ZrN density of 8.26×10^{22} at.cm^{-3}. The as-implanted Eu profile was fitted to a Gaussian function so as to compare with the simulation result.

Fig. 9 shows the measured Eu profile together with simulated Eu profile. The fitted spectrum is also included. The experimental distribution has a projected range that is in agreement within experimental error with the simulated one. The fitted experimental distribution suggests that the simulation is broader. The discrepancies between experimental and simulated distributions are due to the low energy limitations of our accelerator in perfectly resolving the Eu peaks from the ZrN spectrum and the fact that SRIM assumes an amorphous substrate and does not take into consideration the changes that take place during implantation [19].

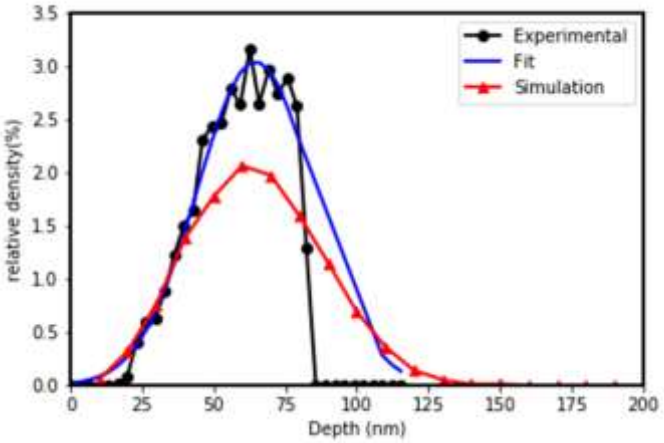

Fig. 9: Europium depth profile in ZrN at room temperature determined by RBS and compared to the theoretical distribution from SRIM-2012.

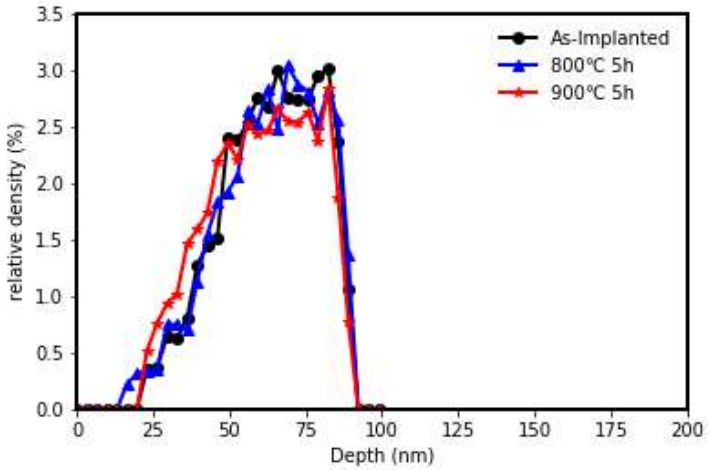

Fig. 10: Europium depth profiles of ZrN implanted at room temperature and isochronically annealed at 800 and 900 °C for 5 hr

Eu depth profiles of annealed and as-implanted samples are shown in Fig. 10. The Eu profiles show negligible change indicating no migration of implanted Eu after annealing at 800 and 900 °C. These results indicate that ZrN could be an effective barrier for Eu at these temperatures. A typical fast-neutron reactors such as a gas-cooled fast reactor operates at an inlet temperature of about 450 °C and an outlet temperature of 850 °C, lower than the annealing temperatures investigated [31]. Though these results are promising for the use of ZrN as a possible diffusion barrier in fast-neutron nuclear reactors, the retainment of Eu by ZrN still needs to be investigated under conditions similar to those in nuclear reactors to validate its applicability in nuclear environment. The retainment of implanted Eu might be the cause of more vacancies retained in the annealed Eu implanted samples as speculated earlier. Doping ZrN with an element heavier than nitrogen such as titanium is known to cause an increase in the acoustic modes [26]. Hence the increase in the acoustic modes in Fig. 7 was due to implanted Eu which also resulted in the formation of N_{Zr} antisites.

Conclusion

Effects of slow and swift heavy ions irradiation of nanocrystalline ZrN deposited onto Si were investigated. The deposited ZrN layers exhibited bands in the Raman spectra of first-order acoustic modes (TA and LA), first-order optic modes (TO and LO), and two more bands between the acoustic and optic modes, which are low-frequency second-order acoustic modes (2A): 2TA and TA+LA. A great amount of radiation defects were observed in the

near-surface of ZrN due to the low-energy irradiation with Eu ions at RT. These defects were characterized by the red-shift and increase in intensity of the TA mode, the blue-shift of the LA mode as well as a significant decrease in the intensity of the first-order optic mode and a general broadening of both the acoustic and optic regions. These defects were attributed to the high nuclear energy loss creating N vacancies. Irradiation with swift Xe ions also caused N vacancies near-surface with less concentration compared to low-energy implantation due to high density of electronic energy loss in the former. Thermal annealing of Eu at 800 and 900 ^{o}C resulted in a reappearance of the LO peak and an increase in the intensity of the TO peak. This was explained to be due to a recombination of N atoms with their vacant sites and formation of N_{Zr} antisite defects. Thermal annealing of Xe irradiated ZrN resulted in an appearance of a new peak between the TA and LA. Generally, thermal annealing resulted in different stoichiometric structures of ZrN different compared to pristine ZrN structure. No migration of Eu in ZrN was observed after annealing at both temperatures. The radiation tolerant and fission product retaining behaviour of fission products such as Eu are promising results for ZrN in nuclear environments.

Acknowledgement

The Authors would like to thanks Prof E Wendler and technical staffs at the Friedrich-Schiller-University Jena, Germany for Eu implantation of the samples.

References

1. *Key World Energy Statistics 2018*. (2018).
2. REFERENCE DATA SERIES (2018). 'Nuclear Power Reactors in the World'. *International Atomic Energy Agency* (2), 79
3. Streit, M. and Ingold, F., (2005). 'Nitrides as a nuclear fuel option'. *Journal of the European Ceramic Society*, *25* (12), pp.2687-2692.
4. Wu, Z., Wu, Y., and Wang, Q., (2019). 'A comparative investigation on structure evolution of ZrN and CrN coatings against ion irradiation'. *Heliyon*, *5*(3), p.e01370.
5. Bao, W., Robertson, S., Liu, J.X., Zhang, G.J., Xu, F. and Wu, H., (2018). 'Structural integrity and characteristics at lattice and nanometre levels of ZrN polycrystalline

irradiated by 4 MeV Au ions'. *Journal of the European Ceramic Society*, *38*(13), pp.4373-4383.

6. Wheeler, K., Peralta, P., Parra, M., McClellan, K., Dunwoody, J. and Egeland, G., (2007). 'Effect of sintering conditions on the microstructure and mechanical properties of ZrN as a surrogate for actinide nitride fuels'. *Journal of nuclear materials*, *366*(3), pp.306-316.
7. Tang, Y., Zhang, G.J., Xue, J.X., Wang, X.G., Xu, C.M. and Huang, X., (2013). 'Densification and mechanical properties of hot-pressed ZrN ceramics doped with Zr or Ti'. *Journal of the European Ceramic Society*, *33*(7), pp.1363-1371.
8. Meyer, M.K., Fielding, R. and Gan, J., (2007). 'Fuel development for gas-cooled fast reactors'. *Journal of Nuclear Materials*, *371*(1-3), pp.281-287.
9. Gribaudo, L., Arias, D., and Abriata, J., (1994). 'The N-Zr (Nitrogen-Zirconium) System'. *Journal of Phase Equilibria*, *15*(4), pp.441–449.
10. Egeland, G.W., (2005). '*Radiation damage and fission product release in zirconium nitride'* (No. LA-14249-T). Los Alamos National Lab.(LANL), Los Alamos, NM (United States).
11. Egeland, G.W., Valdez, J.A., Maloy, S.A., McClellan, K.J., Sickafus, K.E. and Bond, G.M., (2013). 'Heavy-ion irradiation defect accumulation in ZrN characterized by TEM, GIXRD, nanoindentation, and helium desorption'. *Journal of nuclear materials*, *435*(1-3), pp.77-87.
12. van Vuuren, A.J., Skuratov, V., Uglov, V. and Sohatsky, A., (2015). 'Swift heavy ion irradiation effects on He agglomeration in ZrN and TiZrN ceramics'. *The interaction of radiation with a solid,* 156, pp.91-92
13. van Vuuren, A.J., Skuratov, V.A., Uglov, V.V., Neethling, J.H. and Zlotski, S.V., (2013). 'Radiation tolerance of nanostructured ZrN coatings against swift heavy ion irradiation'. *Journal of Nuclear Materials*, *442*(1-3), pp.507-511.
14. Lu, F., Huang, M., Yaqoob, F., Lang, M., Namavar, F., Trautmann, C., Sun, H., Ewing, R.C. and Lian, J., (2012). 'Displacive radiation-induced structural contraction in nanocrystalline ZrN'. *Applied Physics Letters*, *101*(4), p.041904.
15. Craciun, D., Socol, G., Dorcioman, G., Simeone, D., Gosset, D., Behdad, S., Boesl, B., Craciun, V., (2014). 'Ar ions irradiation effects in ZrN thin films grown by pulsed laser deposition'. *Applied Surface Science*, *336*, pp. 129–132.

16. Yang, Y., Dickerson, C. A., and Allen, T. R., (2009). 'Radiation stability of ZrN under 2.6 MeV proton irradiation'. *Journal of Nuclear Materials*, *392*(2), pp. 200–205.
17. Jiao, L., Yu, K.Y., Chen, D., Jacob, C., Shao, L., Zhang, X. and Wang, H., (2015). 'Radiation tolerant nanocrystalline ZrN films under high dose heavy-ion irradiation'. *Journal of Applied Physics*, *117*(14), p.145901.
18. Shah, W.H., Iqbal, Y., Safeen, A., Safeen, K., Khan, G., Shah, W.H., Ahmed, I., Khan, S., Zhao, T. and Ul-Haq, K., (2018). 'Study of the structural and electrical properties of silicon ion irradiated zirconium nitride thin films'. *Modern Physics Letters B*, *32*(24), p.1850281.
19. Ziegler, J.F., Biersack, J.P. and Ziegler, M.D., (2012). SRIM 2008-The Stopping and Range of Ions in Matter, SRIM Co., Chester.
20. Murari, N., Sergo, V., Pezzotti, G., Katagiri, G., Meriani, S. and Nishida, T., (1997). 'Raman piezo-spectroscopic behavior of aluminum nitride'. *Applied spectroscopy*, *51*(11), pp.1761-1765.
21. Kosacki, I., Suzuki, T., Anderson, H.U. and Colomban, P., (2002). 'Raman scattering and lattice defects in nanocrystalline CeO2 thin films'. *Solid State Ionics*, *149*(1-2), pp.99-105.
22. Constable, C.P., Lewis, D.B., Yarwood, J. and Münz, W.D., (2004). 'Raman microscopic studies of residual and applied stress in PVD hard ceramic coatings and correlation with X-ray diffraction (XRD) measurements'. *Surface and Coatings Technology*, *184*(2-3), pp.291-297.
23. Kuznetsov, K.B., Kovalev, I.A., Nechaev, A.N., Ogarkov, A.I., Shevtsov, S.V., Chernyavskii, A.S. and Solntsev, K.A., (2016). 'Stability of the structure of compact zirconium nitride ceramics to irradiation with high-energy xenon ions'. *Inorganic Materials*, *52*(12), pp.1235-1239.
24. Montgomery Jr, G.P., Klein, M.V., Ganguly, B.N. and Wood, R.F., (1972). 'Raman scattering and far-infrared absorption induced by silver ions in sodium chloride'. *Physical Review B*, *6*(10), p.4047.
25. Benedek, G., Nardelli, G.F., (1967). 'Raman Scattering by Colour Centers'. *Phys. Rev.* 154, pp. 872
26. Constable, C.P., Yarwood, J. and Münz, W.D., (1999). 'Raman microscopic studies of PVD hard coatings'. *Surface and Coatings Technology*, *116*, pp.155-159.

27. Spengler, W. and Kaiser, R., (1976). ‘First and second order Raman scattering in transition metal compounds’. *Solid State Communications*, *18*(7), pp.881-884.

28. Klein, M.V., Holy, J.A. and Williams, W.S., (1978). ‘Raman scattering induced by carbon vacancies in Ti C x’. *Physical Review B*, *17*(4), p.1546.

29. Uglov, V.V., Abadias, G., Zlotski, S.V., Saladukhin, I.A., Safronov, I.V., Shymanski, V.I., van Vuuren, A.J., O'Connell, J., Skuratov, V. and Neethling, J.H., (2017). ‘Features of microstructure of ZrN, Si3N4 and ZrN/SiNx nanoscale films irradiated by Xe ions’. *Vacuum*, *143*, pp.491-494.

30. Stoehr, M., Seo, H.S., Petrov, I. and Greene, J.E., (2008). ‘Effect of off stoichiometry on Raman scattering from epitaxial and polycrystalline HfN x (0.85≤ x≤ 1.50) grown on MgO (001)’. *Journal of Applied Physics*, *104*(3), p.033507.

31. Allen, T.R., Sridharan, K., Tan, L., Windes, W.E., Cole, J.I., Crawford, D.C. and Was, G.S., (2008). ‘Materials challenge for generation IV nuclear energy systems’. *Nuclear Technology*, *162*(3), pp.342-357.